# IAEA
INTERNATIONAL ATOMIC ENERGY AGENCY

**20th IAEA Fusion Energy Conference**

**Vilamoura, Portugal, 1-6 November 2004**

# The Confluence of Edge and Core Turbulence and Zonal Flows in Tokamaks

**B. Scott**[1], T. Dannert[1], F. Jenko[1], A. Kendl[2], T. Ribeiro[3], and D. Strintzi[1]

[1]Max-Planck-Institut für Plasmaphysik, EURATOM Association, D-85748 Garching
[2]Institut fuer theoretische Physik, University of Innsbruck, Innsbruck, Austria
[3]CFN-IST, University of Lisbon, Lisbon, Portugal

# The Confluence of Edge and Core Turbulence and Zonal Flows in Tokamaks

**B. Scott**[1], T. Dannert[1], F. Jenko[1], A. Kendl[2], T. Ribeiro[3], and D. Strintzi[1]

[1]Max-Planck-Institut für Plasmaphysik, EURATOM Association, D-85748 Garching
[2]Institut fuer theoretische Physik, University of Innsbruck, Innsbruck, Austria
[3]CFN-IST, University of Lisbon, Lisbon, Portugal
e-mail: bruce.scott@ipp.mpg.de

**Abstract**   We report on gyrofluid and gyrokinetic numerical studies of edge and core turbulence in tokamak geometry, with emphasis on the interaction between spatial regions of differing physical character: core and edge regimes, and the edge/SOL interface. These spatial transitions give a special character to tokamak edge and pedestal dynamics whose study is of fundamental importance to the credible prediction of future reactor performance.

## 1.   Preliminaries

Edge turbulence is characterised by steep gradients [1]: a perp/parallel scale ratio sufficiently extreme that $\hat{\mu} = (m_e/M_i)(qR/L_\perp)^2 > 1$ and hence the drift frequency is larger than the electron transit, $c_s/L_\perp > V_e/qR$, with field line connection length $2\pi qR$ and profile scale length $L_\perp$. It also has $\nu_e > c_s/L_\perp$ and, in modern tokamaks, $c_s/L_\perp > v_A/qR$, making the adiabatic response of the electrons electromagnetic. The latter ratio brings in $\beta_e = c_s^2/v_A^2$ through the drift Alfvén parameter $\hat{\beta} = \beta_e(qR/L_\perp)^2$. The small values of $2L_\perp/R$ de-emphasise interchange and ballooning in favour of a nonlinear electron parallel dynamics. Toroidicity is of crucial importance, on the other hand, in providing energy transfer channels to ExB zonal flows, through their toroidal compression [2,3].

The following were all run within the DALF3 fluid or GEM3 gyrofluid models, unless otherwise indicated (see Secs. 4,6, below). The models are described in Ref. [4]. Briefly, they are four field models treating the vorticity and electron density, and parallel current and ion flow, as dependent variables. The "local" version of each model computes the variables as disturbances on a prescribed background profiles. The GEM3 model also has a "global" version, in which the variables also incorporate the profiles which are maintained by simple sources. The local version uses Dirichlet conditions at both radial (labelled "$x$") boundaries with feedback-controlled source/sink layers to maintain the overall profile (including the zonal averages of the variables). The global version replaces the inner boundary with a Neumann condition on every variable, so that the 2-D Pfirsch-Schlüter equilibrium is also treated self consistently, and the computations are carried long enough to place the entire radial layer in transport equilibrium. In the "global" version, the source at the inner boundary is held fixed, while the sink is still feedback-controlled. Both models work variously with local or global versions of the flux surface geometry as described in Ref. [5]. The numerical scheme is a highly accurate time/space discretisation which (1) preserves the properties of Poisson bracket structures in the spatial derivatives, and (2) is stable to waves and advection, implemented as developed and described by Naulin [6].

It is important to note the utility of the ability to separate toroidicity in the drifts (the "curvature terms") from the coordinate metric from the boundary conditions while maintaining rigorous consistency. This allows the investigation and isolation of physical mechanisms, an important difference between computational physics and modelling.

A well constructed computation will carry the entire scale range from $L_\perp$ to the drift scale $\rho_s$ for all cases. Since for $T_i = T_e$ we have $\rho_s = \rho_i$, i.e., the ion gyroradius, a gyrofluid or gyrokinetic closure with proper energy conservation to all orders in compressional effects (parallel dynamics, curvature terms) becomes necessary. The computation will reflect the "thin atmosphere" property of the edge: the domain size $L_y$ in the electron drift direction (labelled "$y$")

satisfies $L_y \gg L_\perp$ [4]. Moreover, the property of field line connection requires consistency in the parallel direction at the poloidal branch cut [7], so that the domain range of $s$, the parallel coordinate projected onto the poloidal angle, is always $2\pi$.

## 2.  Saturation of Zonal Flows in a Toroidal Magnetic Field

Zonal flows saturate by means of geodesic coupling, involving toroidal compression of a zonal ExB flow, causing its energy to leak into up/down sideband structures in the electron pressure. These sidebands in turn lose energy mainly by being chopped apart by the turbulence and by dumping some of their energy resistively into the Pfirsch-Schlüter current [3]. Note that some of this transfer path is not available to a simplified resistive MHD model, which neglects the coupling between electron pressure and parallel current through the parallel electron dynamics (adiabatic response). It is also important to note that this process features an energy transfer path, not necessarily geodesic acoustic oscillations ("GAMs") per se. The GAM signal itself is found to be relatively weak, not necessarily observable. This is because the turbulence drives the zonal flows via the Reynolds stress incoherently at a wide range of frequencies, into which spectrum the GAM frequency itself falls.

**The slab case**   In a slab model, in which the geodesic curvature is absent, the Reynolds and Maxwell stresses are the only energetic pathways for energy to enter or leave the zonal flows. For typical parameters the Maxwell stress is relatively weak, and saturation can only occur by the Reynolds stress itself becoming small. In contrast to the simplest idea that this should occur only upon complete suppression of the turbulence, it is found that the Reynolds stress spectrum splits into two parts, bordered at $k_y \rho_s \sim 0.3$, with the higher-$k_y$ part driving the flows as the expense of the turbulence and the lower-$k_y$ part *vice versa*. This is consistent with a previous finding that an imposed ExB shear would suppress the short wavelengths but drive at long wavelength if strong enough [8]. Turbulence drives the flow shear until the latter is strong enough, and then the long and short wavelength regions balance. This only occurs at RMS vorticity levels of about $0.5c_s/L_\perp$, while in toroidal geometry the geodesic mechanism, always active, holds the RMS vorticity to levels closer to $0.1c_s/L_\perp$, which is too small to have overwhelming effect on the turbulence.

**Control tests**   Presence/absence tests in which the geodesic mechanism was inserted into the $k_y = 0$ component of the slab case or deleted from the toroidal case. The results from the four cases, considered together, were found to follow according to whether the geodesic mechanism was active, not whether the turbulence itself was slab or toroidal. The main difference was in the mean (zero frequency, lowest $k_x$) flow, with the finite frequency zonal flow spectrum relatively unchanged spatially ($k_x$), although the presence of the geodesic mechanism lead to a broader frequency spectrum. A scaling study [9], varying the geodesic curvature effect on the $k_y = 0$ component from 0 (absent) to 1 (nominal), found the transition to be gradual. Studies of flux surface shaping did not find enhanced zonal flow effects; rather, an enhanced local magnetic shear effect [10,11].

## 3.  Dynamics of the Edge/SOL Interface

The last closed flux surface (LCFS) delineates the interface between the edge and scrape-off layer (SOL) regions of the plasma. The edge region is characterised by edge parameters, specifically $\hat{\mu} > 1$. The closed field lines serve to disallow the presence of a "convective cell (CC) mode" which has $k_\parallel = 0$ at finite $k_y$ [7]. In the SOL, however, the CC modes are present, and due to the lack of parallel dynamics they are found to dominate with interchange mode structure (no cross coherence, phase shifts near $\pi/2$, for $\widetilde{n}_e$ versus $\widetilde{\phi}$). The dynamics under SOL conditions is so strong that local computations with prescribed gradients are no longer tenable.
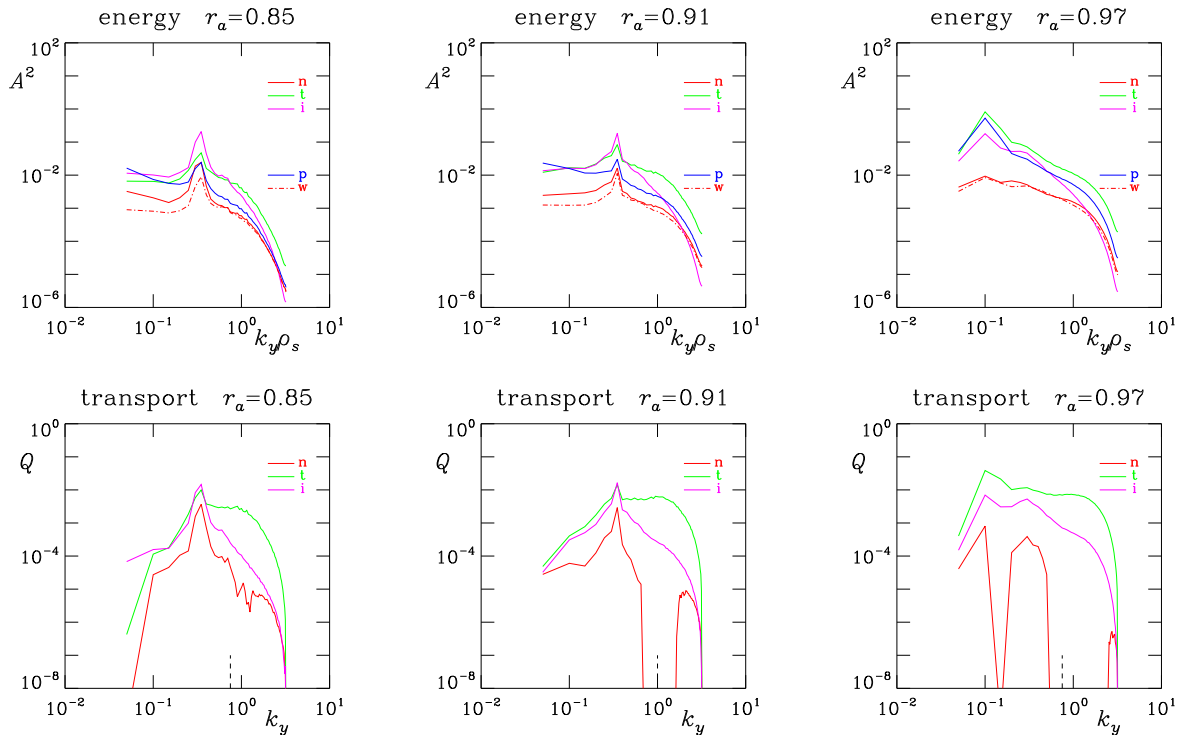
Figure 1: Transition between edge and core turbulence, three locations $r_a = r/a$ on a model profile set, energy and transport spectra (dashed line: median mode for electron thermal transport) as noted in the text. The region $k_y \rho_s \sim 1$ electron shoulder does more transport than the dominant peak.

Hence, the following were all done with a prescribed source, including the zonal component including nominal gradient among the dependent variables.

**Control tests**   Presence/absence tests on the boundary conditions (the SOL case is given a Debye sheath instead of the periodicity constraint on closed flux surfaces) find that the allowance of the CC mode is a drastic qualitative change, turning a situation of drift wave dynamical character into one of more familiar MHD interchange character [12]. The transport in the SOL case increases by a factor of ten, even as the gradient is flattened by a factor of about two, relative to the nominal drift wave case.

**Both edge and SOL regions present**   The GEM3 model was also run with a radially doubled domain, with the outer half given SOL boundary conditions, leaving the inner half as closed flux surfaces. The SOL region was found to affect the dynamics in the edge region. Large scale dynamics which is not found in a pure closed-surface case result, with the ExB shear layer shedding vortices as in a Kelvin-Helmholtz street, the form seen visually in gas-puff imaging experiments [13].

**Poloidal position of the branch cut**   In the above cases the poloidal branch cut was always in the inboard midplane, at $s = \pm\pi$. This was also the position of the limiter in the SOL region. The SOL dynamics was found to be overwhelming either in isolation or in dynamical contact to an edge region. However, when the limiter position was moved to $s = -\pi/2$ (the position of the divertor in modern tokamaks), the direction into which the ions tend to drift, the SOL dynamics was found to be sufficiently weakened that realistic turbulence/transport levels in the SOL resulted.

## 4.   Transition into the Core Regime

The core regime cannot be treated by these four field models, since for small collisionality the passing electrons tend toward adiabaticity, and hence zero particle flux. The ion temperature is necessary. The model used for this is the full version of GEM, the electromagnetic 6-moment model for both species with arbitrary collisionality given in Ref. [10], whose provenance is the core gyrofluid model of Dorland and Hammett [14], extended to toroidal geometry by Beer and Hammett [15]. The model has been corrected for exact energy conservation at all $k_\perp \rho_{i,e}$ in the $\nabla_\parallel$ and curvature terms along the lines of Ref. [4]. This is still the only gyrofluid code treating the temperature dynamics of both species, hence able to treat the edge/core transition while always resolving $\rho_s$ and hence $\rho_i$. The GEM model has also been run for the representative cases covered above, and shows similar dependence upon $\beta_e$ as DALF3 or GEM3 even for turbulence of strong ITG mode structure found for $\eta_i \equiv d\log T_i/d\log n_i > 2$ (cf. Ref. [16] for how the mode structure is determined).

The transition into the core is determined not so much by the collisionality but by the decrease in $R/L_\perp$ from several tens to below ten [10]. This causes both transit frequencies (Alfvén, electron) to become faster than the turbulence. Hence the passing electrons start to drop out of the energetics and the core ITG regime is approached. In most tokamak plasmas, the kinetic ballooning regime [17] is not reached. This situation was treated using three points $r_a = r/a = \{0.97, 0.91, 0.85\}$ on a model profile of varying parameters with differing gradients in all three of $n_e$, $T_e$, and $T_i$. The temperatures extrapolate to zero at $r_a = 1.03$ and $1.12$ for $T_e$ and $T_i$, and are equal (300 eV) at $r_a = 0.85$, while $n_e$ is nearly flat (1.5 at 0.85 and 1.0 at 0.97, units of $10^{13}$ cm$^{-3}$). Other parameters were $B = 2$ T and $q = 4$ and $R_0 = 165$ cm $= 3.3a$ and the shear $\hat{s} = 1$. Selected energy ('n' for $\widetilde{n}_e$, 't' for $\widetilde{T}_e$, 'i' for $\widetilde{T}_i$, 'w' for $\widetilde{\Omega} = \widetilde{n}_e - \widetilde{n}_i$, 'p' for $\widetilde{\phi}$) and ExB transport ('n' for $F_e = \widetilde{n}_e \widetilde{v}_E^x$, 't' for $G_e = \widetilde{T}_e \widetilde{v}_E^x$, 'i' for $G_i = \widetilde{T}_i \widetilde{v}_E^x$, all FLR-corrected) spectra are shown versus $k_y \rho_s$ in Fig. 1. The outermost case, with the most standard edge parameters (e.g., $\hat{\mu} = 13.2$), produced the most obviously electromagnetic, broadband turbulence. A prominent peak occurs at $k_y \rho_s = 0.1$, but the small scale activity is robust enough that the median mode for $G_e$ is 0.75. Evidently the large scale $\nabla T_{e,i}$-driven part sits on a bath of drift waves which fugue into an ETG region for $k_y \rho_i > 1$ (here, $T_i/T_e = 1.5$). This is also seen in the phase shifts which transition sharply from values near $\pi/4$ to $\pm \pi$ as $k_y \rho_i$ increases beyond unity. As the cases transition coreward (towards left, with lower $r_a$), the narrow ITG signal at $k_y \rho_s = 0.3$ becomes clear, but the electron mode bath remains and causes most of the transport. The ratio $G_e/G_i$ is about 3. The trends in normalised units and normalising multipliers nearly cancelled properly, with the electron (ion) transport power in kW given by 188 (31) and 190 (47) and 132 (60), edge to core.

**Meaning of Inhomogeneity**   What is really desired is the ability to vary the parameters across the radial domain of a single case, so that the self consistent adjustment of the profiles will produce a properly divergence free flux and the change in turbulence character will be gradual (or perhaps not). The spatial change of parameters within the computational domain is what is meant by proper inhomogeneity, as opposed to global boundary conditions (allowing zonal profiles of dependent variables to rise or fall) or nonlinearity (ExB advection or magnetic flutter in $\nabla_\parallel$). Inhomogeneity becomes fully nonlinear if the parameters follow from the 3-D spatial variation of the dependent variables. Unfortunately, if the parameters in the equations are simply given radial dependence, no single set of terms among the conservative subsystems will conserve free energy! This is because the parameters no longer commute with $\partial_x$, not even in the parallel dynamics because of the nonlinear magnetic flutter in $\nabla_\parallel$. In the curvature terms the geodesic energy transfer with zonal flows [3] would no longer be conservative, yielding potentially disastrous sources which zonal flows can access.

**A Simple Model for It**    Since fully inhomogeneous gyrofluid equations are not yet ready, we have in the meantime employed a model in which the parallel wave speed in the linear part of $\nabla_\parallel$ is given a radial profile scaling with $V_e(r_a)$ following from the instantaneous zonal average $\langle T_e(r_a) \rangle$. This was run within the GEM model for the edge/SOL situation described for GEM3 above, extended coreward. The radial domain is now $16\,\text{cm}$, with the inner half mostly in the core regime, the third quarter in the edge regime, and the outer quarter a SOL region. This model set heat sources and allowed the profiles to find equilibrium. The $n_e$ profile was allowed to relax as its time scale was longer than the run. The edge-to-core transition was found in the mode structure as $V_e(r_a)/qR$ becomes faster than the turbulence (measured by its RMS vorticity). This model actually produced a pedestal structure in the $\langle T_e(r_a) \rangle$, of width $20\rho_s$. It may be taken as an interesting signpost, but to attain validity this feature should be shown to arise from properly inhomogeneous equations.

## 5.   Fully Nonlinear Gyrofluid Equations

To decide the above question, large computations which are only becoming barely tractable with a well resolved gyrokinetic model are necessary. Severely under-resolved model computations which are now common are not an option. Computation of the full transition into the SOL also generally requires compatibility with arbitrarily large fluctuation amplitude.

To pursue this we have derived a set of gyrofluid equations using field theoretical methods for which an exact energy theorem is found [18]. The energy exchanges between thermal gradient, turbulence, and zonal flows and the shear layer are therefore exactly conservative. In contrast to present-day models this one does not depend on the delta-f approximations, and so (1) radial parameter inhomogeneity becomes compatible with exact energy conservation, and (2) full self consistency among the various elements including heat and particle sources becomes tractable. This work is still in progress (a further paper incorporating both perp and parallel temperatures has been submitted, still another is required before we have the heat fluxes as dynamical variables hence a 6-moment model), but it shows a promising avenue towards the establishment of a fully nonlinear/inhomogeneous model which can reach from global scales down to $\rho_s, \rho_i$ and below. We are also working to incorporate the HELENA code [19] in time dependent fashion, so that the magnetic geometry is allowed to change self consistently with spatial and temporal variations in the plasma parameters.

## 6.   Progress in Gyrokinetic Computation of Edge Turbulence

The nonlinear gyrokinetic description of low frequency dynamics in a magnetised plasma goes back some two decades [20–22], with particle methods being the first practical computational implementation [23,24]. Particle methods were also the first to reach maturity in the standard core turbulence cases treating the passing electrons as in adiabatic parallel force balance [25–28]. Vlasov methods treating the distribution function as a field variable on a grid in a higher dimensional phase space were introduced to treat extreme kinetic phenomena [29–32]. The Vlasov method was then used to treat gyrokinetic instabilities [33], and drift wave turbulence [34,35], as well as ETG turbulence driven by $\nabla T_e$ for $k_y \rho_i > 1$ [36].

Extension of the model to treat edge turbulence includes incorporation of the appropriate coordinate metric techniques to allow slab-character dynamics [5] as well as a suitable collision operator. Moreover, the ability of the numerical scheme to function in the deep MHD regime of the Alfvén dynamics ($k_\perp \sigma_0 \ll 1$ where $\sigma_0$ is the collisionless skin depth, noting that $\sigma_0^2/\rho_s^2 = m_e/\beta_e M_i$) must be ensured since dynamics at the scale of $k_\perp L_\perp \sim 1$ is in this regime. The GENE code [36] has been reworked to improve the capture of collisionless Alfvén wave damping [37], demonstrating this ability for very wide ranges in both $m_e/\beta_e M_i$ and $k_\perp^2 \rho_s^2$. The recurrence problem was addressed, finding that it can be cured with a small hyperviscosity in $v_\parallel$-space

provided the resolution is as large as about 3 or 4 grid nodes per thermal velocity $V_e$. The tail should extend out to about 4 or 5 $V_e$. Hence, at least 32 grid nodes are necessary. The new formulation of GENE is being applied mostly to core turbulence [36], but it is also applicable to the edge, once the above mentioned modifications are made. A separate version, briefly presented herein, has been constructed using the same scheme as in the GEM code.

We note that this is still a delta-f model, in which it is not expected that the parameters vary widely over the radial domain. In terms of Poisson bracket structures, the delta-f gyrokinetic equation solved by the GENE code is

$$\partial_t G + \delta\omega_T F^M \partial_y \psi_e + [\delta\psi, H]_{xy} + [\delta_a\psi + v_\parallel\chi, H]_{xs} - (\mu B)(\chi'/m)[\log B, f]_{sv_\parallel} = C(f) \quad (1)$$

with brackets $[f,g]_{ab} = [(\partial_a f)(\partial_b g) - (\partial_b f)(\partial_a g)]$, generalised potentials

$$\psi_e = J_0\left[\phi - (v_\parallel/c)A_\parallel\right] \qquad\qquad \psi = \psi_e + (1/e)(mv_\parallel^2 + \mu B)\log B \qquad (2)$$

respectively incorporating ExB advection ($\phi$), the magnetic flutter nonlinearity ($A_\parallel$), and curvature and grad-B drift effects ($\log B$), and with inductive and nonadiabatic responses

$$G = f + e(v_\parallel/c)(F^M/T)J_0 A_\parallel \qquad\qquad H = f + e(F^M/T)J_0\phi \qquad (3)$$

where $m$ and $e$ and $T$ and $J_0$ and the background Maxwellian $F^M$ are set for each species. The $sv_\parallel$-bracket is magnetic trapping. The factor of $B$ is understood as constant except for $\log B$ in the curvature and trapping terms. The drift parameters are $\delta = (c/B)$ and $\delta_a = (c/Ba)$, becoming $\delta = \rho_s/L_\perp$ and $\delta_a = \rho_s/a$ in normalised units, where $a$ is the minor radius. The term involving $\omega_T = L_n^{-1} + L_T^{-1}[(mv^2/2T) - 3/2]$, gives the background gradient drive. The quantity $\chi = \chi(x)$ gives the ballistic streaming along unperturbed field lines, with $\chi' \equiv \partial\chi/\partial x = 1/qR$. The factor of $J_0$ is the standard gyroaveraging operator. It is applied in $\mathbf{k}_\perp$-space, with the FFT in the $xy$-plane held consistent with the Dirichlet boundaries in $x$ (the half-wave FFT in $x$ is used). The collision operator $C()$ is a combination of pitch angle scattering in $(v_\parallel, \mu)$ and energy scattering in $(v_\parallel)$, with coefficients set to properly capture the resistive damping of shear Alfvén waves.

Consistent with the above are the field equations, polarisation and induction, given by

$$\sum_{\text{sp}}\int dW \left[eJ_0 f + (J_0^2 - 1)(F^M/T)e^2\phi\right] = 0 \qquad \nabla_\perp^2 A_\parallel + (4\pi/c)\sum_{\text{sp}}\int dW \left[ev_\parallel J_0 f\right] = 0 \quad (4)$$

with the integral over velocity space $\int dW = \int Bd\mu dv_\parallel$ and the sum over species. These equations are solved in $\mathbf{k}_\perp$-space for $\phi$ and $A_\parallel$ in terms of $G$, using the appropriate manipulations following from the definition of $G$.

Fluctuation free energy for this system is analysed in the same manner as in Ref. [24]. The ExB and magnetic energy components are

$$\mathcal{E}_E = (1/2)\sum_{\text{sp}}\int d\Lambda (1 - J_0^2)(F^M/T)e^2\phi^2 \qquad\qquad \mathcal{E}_M = (1/8\pi)\int dV\, k_\perp^2 A_\parallel^2 \qquad (5)$$

where $\int dV$ denotes the integral over space (a 3-D average over grid nodes) and $\int d\Lambda$ over phase space (5-D average), and the $k_\perp$-based operators are evaluated in $\mathbf{k}_\perp$-space. Using Eqs. (4) the time derivatives of these become

$$\partial_t \mathcal{E}_E = \sum_{\text{sp}}\int d\Lambda\, eJ_0\phi\,\partial_t f \qquad\qquad \partial_t \mathcal{E}_M = \sum_{\text{sp}}\int d\Lambda\, ef(v_\parallel/c)J_0\,\partial_t A_\parallel \qquad (6)$$
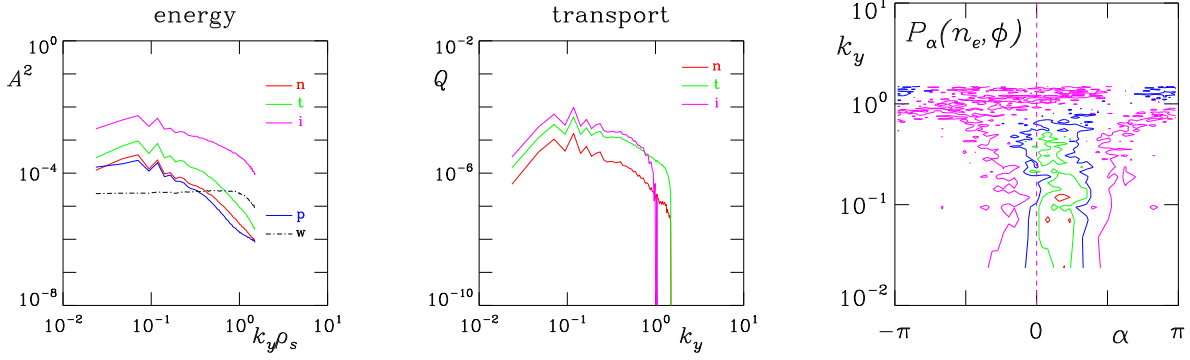
Figure 2: Spectra and phase shifts from the collisional/edge version of the GENE code, for a standard ITG edge case as explained in the text. Every feature is as found in the GEM model, except (not shown) a very small, but positive, transport of tail electrons radially along fluctuating magnetic field lines.

The free energy contained in $f$ itself and its time derivative are

$$\mathcal{E}_F = (1/2) \sum_{\text{sp}} \int d\Lambda \, (T/F^M) f^2 \qquad \partial_t \mathcal{E}_F = \sum_{\text{sp}} \int d\Lambda \, (T/F^M) f \partial_t f \qquad (7)$$

related to the entropy in the fluctuations. Combining these three pieces we find the conservation theorem for Eqs. (1,4),

$$\sum_{\text{sp}} \int d\Lambda \frac{T}{F^M} H \frac{\partial G}{\partial t} = \sum_{\text{sp}} \int d\Lambda \left[ -v_\parallel \chi' \frac{\partial (\log B)}{\partial s} \frac{\mu B}{F^M} \frac{f^2}{2} - \delta \omega_T T f \frac{\partial \psi_e}{\partial y} + \frac{T}{F^M} f C(f) \right] \quad (8)$$

with the magnetic trapping, gradient drive appearing as (potential) sources, and collisional dissipation as a sink. The components of this energy theorem can be used to diagnose the physical processes in the GENE model in the same manner as for GEM/3 and DALF3 [4].

The standard case run with this model is $qR/L_T = 100$ and $\beta_e = 10^{-4}$ and $\nu_e L_T/c_s = 1$ and $R/L_T = 30$ and $L_n = 2L_T$ with same $L_T$ for $(e,i)$ and $\delta = 10\delta_a = 0.015$, run into saturation (start amplitude $10^{-4}$, linear overshoot at $t = 50$, saturation after 200, run to 800, with times in units of $L_T/c_s$ here and below). Selected energy and transport spectra are shown in Fig. 2 (as in Fig. 1, with vorticity $\widetilde{\Omega} = \int dW [f_e - f_i]$), together with the phase shift distributions for $\widetilde{n}_e$ ahead of $\widetilde{\phi}$ for each $k_y$. As in the GEM and GEM3 results, $\widetilde{\Omega}$ is flat out to $k_y\rho_s = 1$, the amplitudes peak at long wavelength, and the transport also at long wavelength but with a significant component coming from the $0.3 < k_y\rho_s < 1$ nonlinear drift wave range where the density of states is higher. There is no particular role for the scale of the dominant linear instability, an ITG-type mode at $k_y\rho_s = 0.2$, and the correlation lengths are not found to follow the linear scales, even in scaling studies (neither DALF3/GEM3 nor GEM nor GENE finds this in edge turbulence, underscoring the need to carry the entire scale range). Radial correlation lengths are almost always in the range 5-7$\rho_s$ irrespective of $\nu_e$ or $\beta_e$, until the beta limit (low-$k_y$ ideal ballooning) is reached. Scalings are being done for $\beta_e$ and $\nu_e$, increasing each in a separate run by a factor of $(t - 800)/800$ after 800, to be reported at the conference.

**The full-f FEFI model**  Except for the fact that magnetic trapping is treated by GENE, applying the GENE model to a spatial edge/core transition would encounter similar problems as with GEM: it is a local model not intended for strongly inhomogeneous parameter situations. Although computation in gyrokinetics is more intensive than in gyrofluid models, it has been

found easier to extend the numerical scheme to the global situation in gyrokinetics, since the treatment of $f$ in $d\Lambda$ is already general. It remains only to relax linearity in the wave trapping and polarisation. A way has been found to do this to high accuracy, incorporating full nonlinear collisions and trapping so that energy is conserved by trans-collisional Alfvén dynamics within $10^{-6}$ over a transport time scale. This model, called FEFI (full electrons, full ions), will be reported in detail in the near future. At the time of this writing, the nonlinear brackets and the elliptic solver required for the full nonlinear versions of Eqs. (4) are still being incorporated. But it is expected that several runs, parallelised over 256 PEs running for about 100 hr each, will be able to elucidate the full nonlinear, kinetic physics of the edge/core transition. Using the global version of Ref. [5] the general tokamak geometry can be incorporated at no additional cost, but for generic studies (esp. benchmarks) this is neither necessary nor desirable. But substantial progress can be expected on this and the above fronts in the very near future.

## 7.   Testing Other Models

The versions of these codes with global boundary conditions will be used as well to test general paradigms such as the predator/prey scenarios for ExB shear flow [38] and trapped ion effects on flow layers [39], including collisions [40,41], in the presence of fully developed, well resolved turbulence at arbitrary collisionality. In some cases the models are constructed for simple dynamics, and so DALF3 is germane (GEM3 for warm ions), not least as a relaxation of the very restrictive cases with under-resolved resistive-g used to underpin the generic fluid scenarios. In others the full FEFI model is necessary to treat both equilibrium and turbulence on a kinetic level. The key thrust in all cases, however, is full resolution and self consistency, which is required for any result to be robustly viable.

**References**
 [1]   SCOTT, B., Plasma Phys. Controlled Fusion **39** (1997) 1635.
 [2]   HALLATSCHEK, K. et al., Phys. Rev. Lett. **86** (2001) 1223.
 [3]   SCOTT, B., Phys. Lett. A **320** (2003) 53.
 [4]   SCOTT, B., Plasma Phys. Controlled Fusion **45** (2003) A385.
 [5]   SCOTT, B., Phys. Plasmas **8** (2001) 447.
 [6]   NAULIN, V., Plasma Phys. **10** (2003) 4016.
 [7]   SCOTT, B., Phys. Plasmas **5** (1998) 2334.
 [8]   SCOTT, B., Plasma Phys. Controlled Fusion **34** (1992) 1977.
 [9]   KENDL, A. et al., Phys. Plasmas (2004) submitted.
[10]   SCOTT, B., Phys. Plasmas **7** (2000) 1845.
[11]   KENDL, A. et al., Phys. Rev. Lett. **90** (2003) 035006.
[12]   RIBEIRO, T. et al., Phys. Plasmas (2004) submitted.
[13]   ZWEBEN, S. J. et al., Nucl. Fusion **44** (2004) 134.
[14]   DORLAND, W. et al., Phys. Fluids B **5** (1993) 812.
[15]   BEER, M. et al., Phys. Plasmas **3** (1996) 4046.
[16]   SCOTT, B., New J. Phys. **4** (2002) 52.
[17]   SNYDER, P. et al., Phys. Plasmas **8** (2001) 744.
[18]   STRINTZI, D. et al., Phys. Plasmas **11** (2004) in press.
[19]   HUIJSMANS, G., *External resistive modes in tokamaks*, PhD thesis, V. Uni. Amsterdam, 1991.
[20]   FRIEMAN, E. A. et al., Phys. Fluids **25** (1982) 502.
[21]   HAHM, T. S. et al., Phys. Fluids **31** (1988) 1940.
[22]   BRIZARD, A., Phys. Fluids B **1** (1989) 1381.
[23]   LEE, W. W., Phys. Fluids **26** (1983) 556.
[24]   LEE, W. W. et al., Phys. Fluids **31** (1988) 612.
[25]   DIMITS, A. M. et al., J. Comput. Phys. **107** (1993) 309.
[26]   PARKER, S. E. et al., Phys. Fluids B **5** (1993) 77.
[27]   SYDORA, R. D., Physica Scripta **52** (1995) 474.
[28]   LIN, Z. et al., Science **281** (1998) 1835.
[29]   CHENG, C. Z. et al., J. Comput. Phys. **22** (1976) 330.
[30]   GAGNE, R. et al., J. Comput. Phys. **24** (1977) 445.
[31]   GHIZZO, A. et al., Phys. Fluids **31** (1988) 72.
[32]   BERTRAND, P. et al., Phys. Fluids B **2** (1990) 1028.
[33]   KOTSCHENREUTHER, M. et al., Comput. Phys. Comm. **88** (1995) 128.
[34]   JENKO, F. et al., Phys. Rev. Lett. **80** (1998) 4883.
[35]   JENKO, F. et al., Phys. Plasmas **6** (1999) 2705.
[36]   JENKO, F. et al., Phys. Plasmas **7** (2000) 1904.
[37]   DANNERT, T. et al., Comput. Phys. Comm. (2004) in press.
[38]   DIAMOND, P. H. et al., Phys. Rev. Lett. **72** (1994) 2565.
[39]   ROSENBLUTH, M. N. et al., Phys. Rev. Lett. **80** (1998) 724.
[40]   LIN, Z. et al., Phys. Rev. Lett. **83** (1999) 3645.
[41]   FALCHETTO, G. L. et al., Phys. Rev. Lett. **92** (2004) 025002.